Journal of Organometallic Chemistry, 384 (1990) 405–415
Elsevier Sequoia S.A., Lausanne – Printed in The Netherlands
JOM 20492

Molecular orbital analysis of mono- and di-carbido-gold cluster compounds

D. Michael P. Mingos * and René P.F. Kanters

Inorganic Chemistry Laboratory, University of Oxford, South Parks Road, Oxford OX1 3QR (U.K.)

(Received September 9th, 1989)

Abstract

The bonding in mono- and di-carbido clusters of gold have been analysed through semi-empirical molecular orbital calculations. The mono-carbido clusters $[C(AuPH_3)_m]$ are characterised by $12m + 8$ valence electrons, and the radial bonding interactions between the carbon and gold atoms predominate. The bonding in related clusters with interstitial boron and nitrogen is also described. In the dicarbido clusters $[C_2(AuPH_3)_m]$ ($m = 8$, 10 or 12) alternative closed shell electron counts are possible. Clusters with $12m + 10$ valence electrons are predicted to be stable and to have short C–C distances resulting from C–C multiple bonding. In the clusters with $12m + 14$ valence electrons the C–C distance is likely to be a very sensitive function of the polyhedral geometry. A bonded C_2 moiety will be observed only if it is compatible with the formation of Au–C bonds of ca 2.0 Å to adjacent gold atoms. Dicarbido-clusters with $12m + 16$ electrons are predicted to be unstable relative to monocarbido clusters.

Introduction

In 1976 molecular orbital calculations were reported for a series of gold cluster compounds of the general type $[(AuPR_3)_n]^{x+}$ and $[Au(AuPR_3)_n]^{x+}$ [1] which defined their closed shell electronic requirements and structural preferences. As part of this investigation the bonding in the octahedral cluster $[(AuP(p\text{-tolyl})_3)_6]^{2+}$ (p-tolyl = 4-methylphenyl), whose crystal X-ray structure had been reported by Bellon et al. [2], was analysed. It was established that this formulation resulted in an open shell structure with two electrons occupying a t_{1u} set of molecular orbitals. It was argued that a much more stable ion would result if the gold cluster contained an interstitial carbido-ligand which would be capable of donating four electrons to complete the occupancy of the t_{1u} set of molecular orbitals. In 1988 Schmidbaur et al. [3] confirmed the validity of this theoretical prediction by synthesising $[C(AuPPh_3)_6]^{2+}$ and structurally characterising it. They also demonstrated that the

0022-328X/90/$03.50

X-ray data of Bellon et al. [2] were consistent with the formulation $[C(AuP(p\text{-tolyl})_3)_6]^{2+}$. Subsequently, Schmidbaur et al. [4] reported the synthesis and characterisation of $[C(AuPPh_3)_5]^+$, which has a trigonal bipyramidal cluster geometry.

The resurgence of interest in this class of compound arising from Schmidbaur's results has prompted us to complete a more detailed molecular orbital analysis of gold cluster compounds with interstitial main group atoms and also to investigate the possibility of defining the closed shell requirements for gold clusters containing dicarbido interstitial fragments. These analyses draw heavily on the previous molecular orbital studies which we have completed on gold cluster compounds [5–8] and on dicarbidometal carbonyl clusters [9]. The mode of calculation and the parameters used are very similar to those used in these previous studies.

Results and discussion

Interstitial main group atom gold clusters

Molecular orbital calculations on the isoelectronic series of ions $[B(AuPH_3)_6]^+$, $[C(AuPH_3)_6]^{2+}$ and $[N(AuPH_3)_6]^{3+}$ containing interstitial atoms were completed. In each case an idealised octahedral metal skeletal geometry was assumed, with the central atom–Au distance equal to 2.20 Å. The molecular orbitals for octahedral $[(AuPH_3)_6]$ are illustrated on the left hand side of Fig. 1. The Au–P σ-bonds and the *d*-band containing 30 closely spaced molecular orbitals are readily discernable. The gold–gold bonding arises primarily from the $a_{1g}(S^\sigma)$ and $t_{1u}(P^\sigma)$ molecular orbitals which occur at slightly higher energies than the gold *d*-band. Complete occupation of these molecular orbitals would require a negatively charged cluster $[(AuPH_3)_6]^{2-}$, and since all known gold clusters of this type bear a positive charge this does not represent a realistic possibility. $[(AuPH_3)_6]^{4+}$ represents a more realistic situation and corresponds to the occupation of only the $a_{1g}(S^\sigma)$ molecular orbital. An incompletely filled $t_{1u}(P^\sigma)$ would be associated with a significant distortion of the skeletal geometry. We have demonstrated elsewhere [10], that the configuration $(S^\sigma)^2(P^\sigma)^4$ would result in an oblate geometry, e.g. a pentagonal pyramid, and $(S^\sigma)^2(P^\sigma)^2$ a prolate geometry. A single crystal X-ray study of $[Au_6(PPh_3)_6]^{2+}$ $[(S^\sigma)^2(P^\sigma)^2]$ has established [11] such a prolate geometry based on two tetrahedra sharing an edge. Reference 5 gives a detailed molecular orbital analysis which accounts for the observation of this geometry in preference to an octahedral geometry.

The effect of introducing an interstitial atom into the octahedral $[(AuPH_3)_6]$ cluster is illustrated in Fig. 1. The main group atoms B, C and N have $2s$ and $2p$ valence orbitals which match the $a_{1g}(S^\sigma)$ and $t_{1u}(P^\sigma)$ skeletal molecular orbitals of the cluster and lead to their stabilisation. The relevant overlap populations between these orbitals are summarised below:

	B	C	N
a_{1g}–$2s$	0.74	0.52	0.35
t_{1u}–$2p$	0.68	0.57	0.39

They indicate a steady decrease from B to N for both $2s$ and $2p$. This results from a contraction of the $2s$ and $2p$ orbitals as the effective nuclear charge increases. The orbital interaction diagram in Fig. 1 represents the situation for $[C(AuPH_3)_6]^{2+}$. In

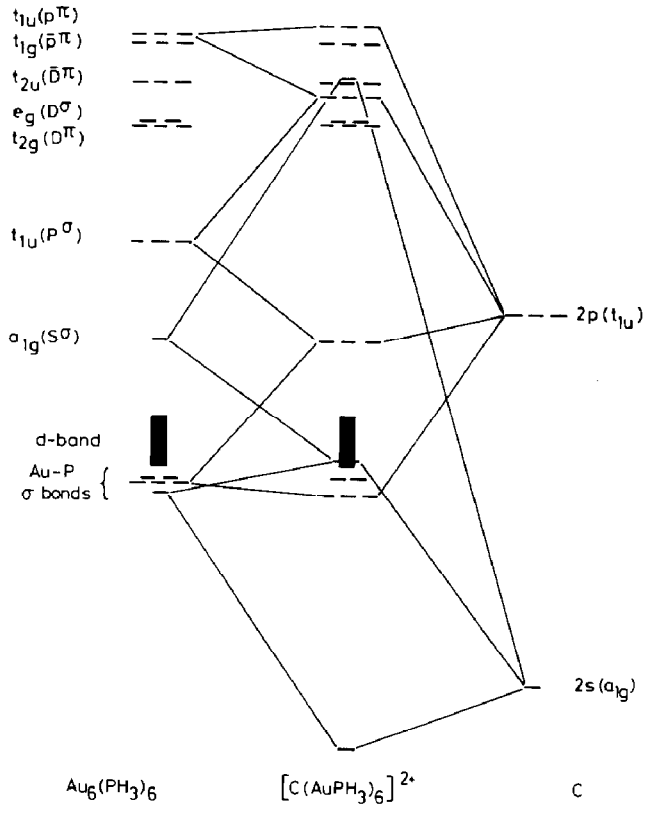

Fig. 1. Orbital interaction diagram for $[C(AuPH_3)_6]^{2+}$, showing the important bonding interactions of the C $2s$ and $2p$ orbitals with the skeletal molecular orbitals of the gold cluster.

the related boron and nitrogen compounds the energies of the $2s$ and $2p$ orbitals are displaced in a manner which reflects the relative electronegativities of B, C and N. In each case a strong interaction occurs and results in substantial stabilisation of the a_{1g} and t_{1u} molecular orbitals A large HOMO-LUMO gap is observed for these ions.

The in-phase combination of the $2s$–$a_{1g}(S^{\sigma})$ and $2p$–$t_{1u}(P^{\sigma})$ molecular orbitals in $[E(AuPH_3)_6]$ are illustrated below in Scheme 1. It is noteworthy that there is a significant contribution from the metal d-orbitals. The $2p$–$t_{1u}(P^{\sigma})$ molecular orbital has σ- and π-bonding components, and in metal-carbonyl carbido-clusters the π-component is significant [12]. In these gold cluster compounds the π-component is not significant; the π overlap population between the $2p_z$–$5d_{xz}$ is effectively zero and between $2p_z$–$6p_z$ only 0.01.

The strong interactions between the $2s$ and $2p$ orbitals of the main group atom and skeletal molecular orbitals of the cluster results in a major redistribution of bonding electron density. This is apparent from Table 1, which summarises the overlap populations for these compounds and allows a comparison with those in the uncentered clusters. It is particularly noteworthy that the gold–gold bonding is almost completely replaced by strong radial Au–E (E = B, C or N) bonding. The bonding interactions are strongest for E = B, where there is a particularly good overlap and energy match between the $2s$ and $2p$ orbitals and the $a_{1g}(S^{\sigma})$ and

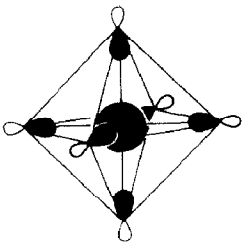

$2s - a_{1g}(S^{\sigma})$

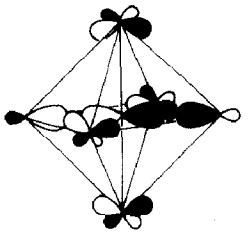

$2p_x - t_{1u}(P_x^{\sigma})$

Scheme 1

$t_{1u}(P^{\sigma})$ skeletal molecular orbitals. These radial interactions also influence the Au–P bonds, which are significantly stronger in the clusters containing interstitial atoms. As the electronegativity of the interstitial atom increases the bonding molecular orbitals derived from in-phase combinations of $2s$–$a_{1g}(S^{\sigma})$ and $2p$–$t_{1u}(P^{\sigma})$ become more localised on the interstitial atom, and the computed negative charge on this atom increases accordingly (see Table 1).

Molecular orbital calculations have also been completed on the related trigonal bipyramidal $[E(AuPPh_3)_5]$ and tetrahedral $[E(AuPPh_3)_4]$ clusters. In each case the most stable closed shell configuration is associated with $12m + 8$ valence electrons, where m is the number of gold atoms. This corresponds to the filling of the S^{σ} and P^{σ} radial Au–E bonding molecular orbitals. Table 2 summarises the results of molecular orbital calculations on tetrahedral, trigonal bipyramidal and octahedral carbido-clusters with $12m + 8$ valence electrons. In each example, the metal–carbon radial bonding predominates, and the gold–gold bonding is extremely weak. The Au–C overlap population decreases as the number of gold atoms increases, but the total bonding effect is greater since there are more Au–C bonds. The computed negative charge decreases with the nuclearity of the cluster reflecting the greater degree of electron delocalisation.

Table 1

Comparison of the overlap populations and charges for $[E(AuPH_3)_6]^{m+}$ (E = B, C and N), $[(AuPH_3)_6]^{4+}$ and $[(AuPH_3)_6]^{2-}$

	Overlap populations			Charges		
	Au–Au	Au–E	Au–P	Au	E	P
$[(AuPH_3)_6]^{2-}$	0.157		0.297	−0.66		0.33
$[(AuPH_3)_6]^{4+}$	0.089		0.378	0.24		0.42
$[B(AuPH_3)_6]^{+}$	0.038	0.505	0.359	−0.10	−0.62	0.37
$[C(AuPH_3)_6]^{2+}$	0.026	0.406	0.403	0.10	−1.07	0.42
$[N(AuPH_3)_6]^{3+}$	0.022	0.273	0.423	0.25	−1.20	0.45

Table 2

Summary of computed overlap populations and charges for $[C(AuPH_3)_m]^{(m-4)+}$

		Overlap populations					Charges
		Au–Au	Au–E	Au–P	Au	E	P
$[C(AuPH_3)_4]$		−0.012	0.551	0.401	−0.04	−1.47	0.41
$[C(AuPH_3)_5]^+$	ax−eq	0.028	0.424	0.404	0.08		0.42
	eq−eq	−0.013	0.494	0.401	0.07	−1.25	0.41
$[C(AuPH_3)_6]^{2+}$		0.026	0.406	0.403	0.10	−1.07	0.42

The bonding analysis presented above for $[E(AuPH_3)_n]$ emphasises the advantages of using the Tensor Surface Harmonics method, which stresses the spheroidal nature of the bonding problem, rather than the point group symmetries of the individual clusters. We have previously demonstrated that for all deltahedral clusters based on $AuPH_3$ fragments the most stable molecular orbitals correspond to S^σ and a set of three P^σ molecular orbitals which are singly nodal. These molecular orbitals always match the symmetries of the $2s$ and $2p$ valence orbitals of the central main group atom and generate a set of very stable S^σ and P^σ molecular orbitals delocalised over the cage and the main group atom. Therefore, such molecules are always characterised by $12m + 8$ valence electrons. Known examples which conform to this generalisation include: $[Cl(AuPPh_3)_2]^+$ [13], $[E(AuPPh_3)_3]^+$ (E = O [14], S or Se [15]), $[N(AuPPh_3)_4]^+$ [16], $[C(AuPPh_3)_5]^+$ [4] and $[C(AuPPh_3)_6]^{2+}$ [3].

The larger Au–E overlap populations for the less electronegative atom (Table 1) suggest that the coordination number of these clusters are influenced by the electronegativity of the central atom. We have also made estimates of the total stabilisation energies for the following aggregation reactions:

$$[E(AuPH_3)_4]^{x+} + AuPH_3^+ \rightleftharpoons [E(AuPH_3)_5]^{(x+1)+}$$

$$[E(AuPH_3)_5]^{(x+1)+} + AuPH_3^+ \rightleftharpoons [E(AuPH_3)_6]^{(x+2)+}$$

The relative stabilities of the higher coordination number clusters fall in the order B > C > N > O. The compounds of this type which have been isolated and are summarised above bear out this generalisation. These results indicate that gold cluster compounds with interstitial boron atoms should be particularly stable and may have coordination numbers greater than those currently observed for O, N and C. Specifically, $[B(AuPH_3)_6]^+$ and $[B(AuPH_3)_7]^{2+}$ should be stable cluster cations.

Extended Hückel calculations cannot always be used reliably to estimate bond lengths in molecules, nonetheless we have carried out some calculations aimed at evaluating the influence of E on the E–Au bond length in these octahedral clusters. In $[C(AuPH_3)_6]^{2+}$ the energy minimum corresponded to a C–Au distance of 2.10 Å, which is close to that determined experimentally (2.12 Å). Similar distances were computed for $[B(AuPH_3)_6]^+$ and $[N(AuPH_3)_6]^{3+}$, suggesting that the cluster does not expand or contract greatly when the interstitial atom is replaced by another atom from the same row of the Periodic Table.

Dicarbido gold cluster compounds

In a previous paper [9] we have defined the geometrical constraints associated with placing a dicarbido-(C_2) ligand inside either a single polyhedron or a pair of

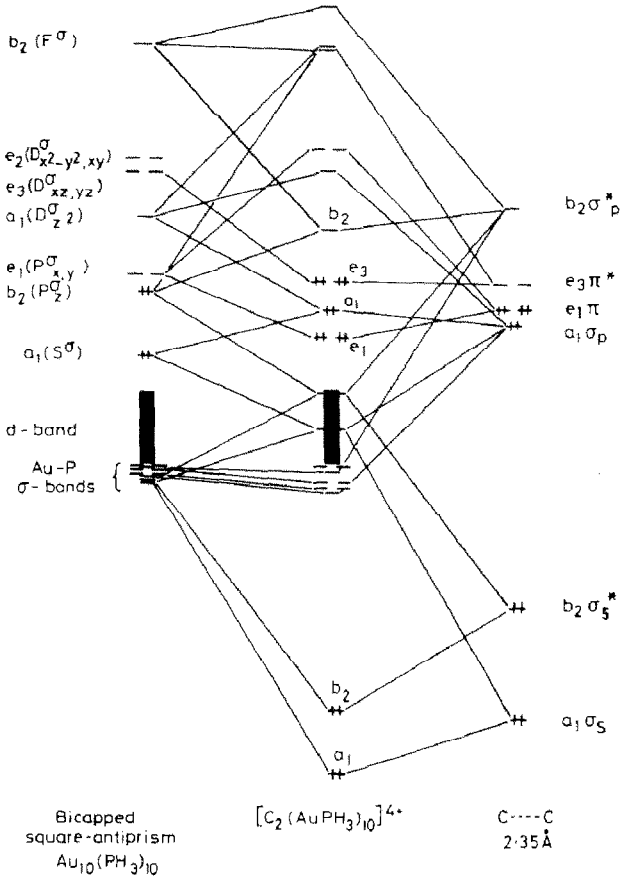

Fig. 2. The interaction diagram for a C_2 fragment within a bicapped square antiprism. The orbital occupations refer to $[C_2(AuPH_3)_{10}]^{4+}$ with $12n_s + 14$ valence electrons.

condensed polyhedra. In particular, a pair of trigonal prisms sharing a common square face leads to a centroid–centroid distance of 1.62 Å if the metal–metal bond lengths are 2.80 Å in length. This corresponds approximately to a C–C single bond. In contrast, the centroid–centroid distance between a pair of square antiprisms sharing a square face is 2.36 Å for the same metal–metal distance. Therefore, if the carbon atoms occupy these positions this would correspond to a dissociation of the C_2 fragment. There remains, however, the possibility of the carbon atoms moving closer together if the C–C bonding were stronger than the metal carbon bonding. In addition, the size of the cavity for the larger deltahedra, e.g. a bicapped square antiprism and an icosahedron, becomes sufficiently large to accommodate a C_2 fragment. We have completed molecular orbital calculations on all of these systems in order to throw some light on the possibility of stabilising C_2 units within a gold phosphine cluster and also to predict the closed shell requirements for such cluster compounds.

Figure 2 illustrates the interaction diagram for a C_2 fragment within an $[(AuPH_3)_{10}]$ cluster with a bicapped square antiprismatic geometry. Initially the carbon atoms were located in the four atom planes of gold atoms which corresponds to a C–C distance of 2.35 Å. On the right hand side of the figure the molecular

orbitals for the C_2 moiety are shown. At a C–C distance of 2.35 Å the π and $\pi^\star$ and σ and $\sigma^\star$ molecular orbitals are closely spaced because the C–C overlap integrals are not large. We have previously noted that [9] the C_2 fragment enters into forward and back donation interactions with the skeletal molecular orbitals of a metal cluster. In particular, in $[C_2(AuPH_3)_{10}]^{4+}$ the π orbital of C_2 donates 1.97 electrons and the $\pi^\star$ orbital accepts 2.54 electrons from the skeletal molecular orbitals. The remaining orbitals involve less electron transfer; approximately 0.6 $\bar{e}$ for σ_p, $\sigma_s^\star$ and σ_s and 0.23 $\bar{e}$ for $\sigma_p^\star$. The dicarbido fragment therefore only has a net charge of -1.14 $\bar{e}$ in the cluster $[C_2(AuPH_3)_{10}]^{4+}$ and the bonding is best described within a delocalised framework.

On the left hand side of Fig. 2 the skeletal molecular orbitals of the bicapped square antiprismatic cluster are shown. The bonding skeletal molecular orbitals are $a_1(S^\sigma)$, $e_1(P^\sigma_{x,y})$ and $b_2(P^\sigma_z)$ and the lowest lying antibonding radial skeletal molecular orbitals are $a_1(D^\sigma_{z^2})$, $e_3(D^\sigma_{xz,yz})$ and $e_2(D^\sigma_{x^2-y^2,xy})$. At higher energies there are the $b_2(F^\sigma)$ and L^π tangential molecular orbitals. The π-orbitals of C_2 interact strongly with the $e_1(P^\sigma_{x,y})$ skeletal bonding molecular orbitals and the $\pi^\star$-orbital with the antibonding $e_3(D^\sigma_{xz,yz})$ skeletal molecular orbitals. These interactions are represented schematically in Scheme 2. The σ_p and σ_s C–C bonding molecular orbitals both have a_1 symmetry and enter into bonding interactions with the $a_1(S^\sigma)$ and $a_1(D^\sigma_{z^2})$ skeletal molecular orbitals. The $\sigma_s^\star$ molecular orbital interacts in a bonding manner with $b_2(P^\sigma_z)$, but these interactions are complicated by the presence of $\sigma_p^\star$ which also has b_2 symmetry. The orbital of b_2 symmetry in the frontier orbital region is out-of-phase between $b_2(P^\sigma_z)$ and $\sigma_p^\star$ but in-phase with respect to $b_2(F^\sigma)$. This interaction is represented schematically in Scheme 3. This molecular orbital lies in the frontier orbital region between the bonding $\pi^\star$–$e_3(D^\sigma_{xz,yz})$ molecular orbitals and the anti-bonding σ_p–$a_1(S^\sigma)$ molecular orbitals in Fig. 2.

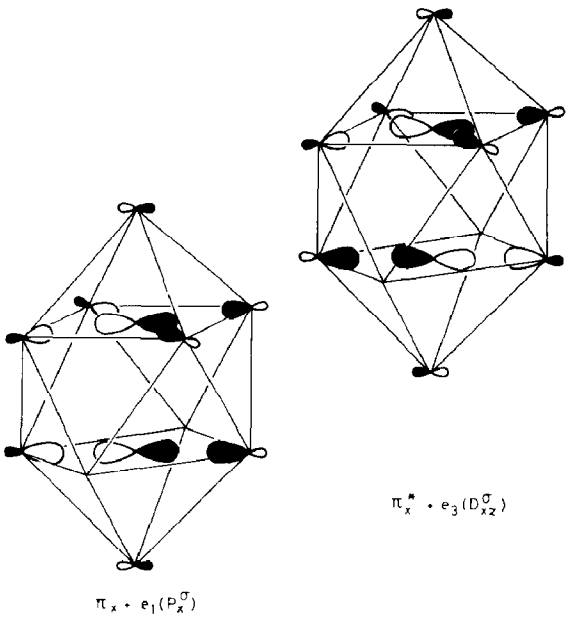

Scheme 2

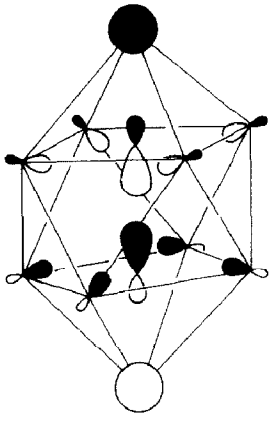

$b_2 \cdot F_{2^3}^{\sigma}$

Scheme 3

The presence of this b_2 molecular orbital leads to two alternative closed shell electronic configurations. If the b_2 molecular orbital remains vacant the highest occupied molecular orbital is e_3 and there is a HOMO-LUMO gap of 1.42 eV, whereas if it is populated a HOMO-LUMO gap of 1.62 eV exists. If 12 valence electrons are associated with the d shell and metal-ligand σ-bond of each of the $AuPH_3$ fragments this corresponds to two alternative electron counts of $12 \times 10 + 14 = 134$ and $12 \times 10 + 16 = 136$.

We have previously established [8] that high nuclearity cluster compounds, in which the radial bonding predominates, have closed shell electronic configurations of $12n_s + \Delta_i$ electron (n_s is the number of surface metal atoms and Δ_i is the electron count associated with the interstitial moiety). In these clusters the interstitial moiety is a C_2 fragment for which the characteristic electron count is 16 if the carbon atoms are well separated and 14 if the carbon atoms are sufficiently close to be represented by a single bond. In localised orbital terms this corresponds to filling all the C–C molecular orbitals including $\sigma_p^{\star}$ (16 electrons) or leaving this orbital vacant (14 electrons). The ambiguity in electron count for the $[C_2(AuPH_3)_{10}]$ cluster is closely related to this phenomenon, because the frontier orbital which is populated to achieve the higher electron count is derived from $b_2(\sigma_p^{\star})$. This orbital, however, is not localised exclusively on the carbon atoms but also has contributions from the skeletal molecular orbitals.

For $[C_2(AuPH_3)_{10}]^{4+}$, with $12n_s + 14$ valence electrons the C–C overlap population is 0.13 which indicates only a weak interaction between the carbon atoms. The Au–Au overlap populations are between 0.050 and 0.076 and approximately the same as those noted previously for the octahedral carbido-cluster. The Au–C bonding interactions are the most important in these molecules and the relevant overlap populations are 0.399 to the capping gold atoms and 0.485 to the square antiprismatic gold atoms.

We have also investigated the effects of bringing the two carbon atoms closer together whilst keeping the metal–metal bond lengths of the bicapped square antiprismatic cluster at 2.80 Å. The relevant Walsh diagram for the C–C compres-

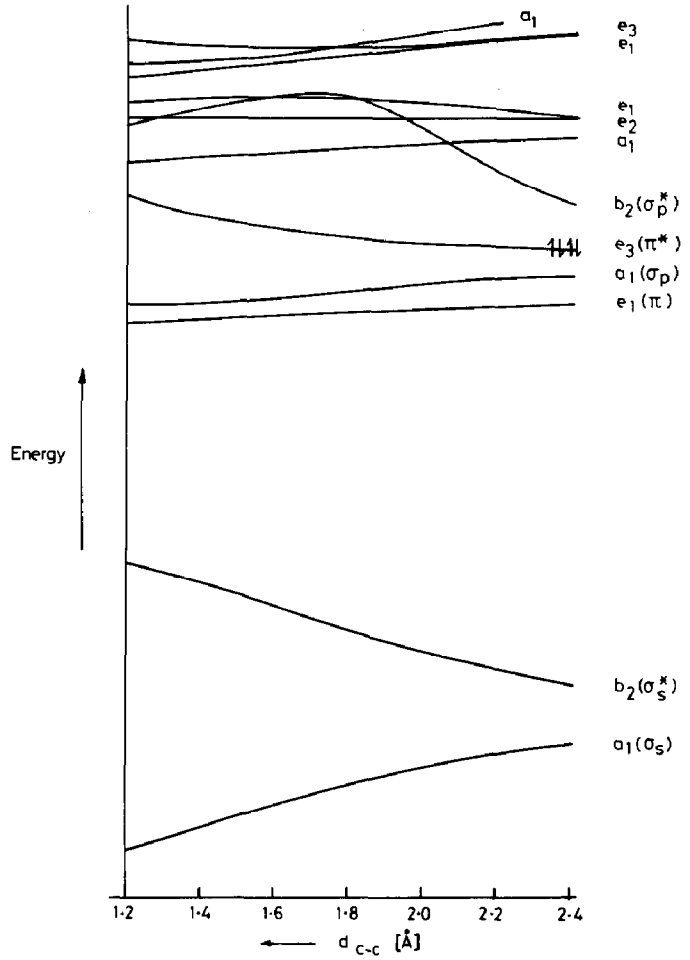

Fig. 3. Walsh diagram for variation of the C–C distance within the bicapped square antiprismatic cluster $[C_2(AuPH_3)_{10}]^{4+}$. The highest occupied orbital in this ion is indicated by pairs of arrows. For reasons of clarity the metal *d* band and metal–phosphorus σ-bonds are not shown.

sion is illustrated in Fig. 3. Interestingly even for the $12n_s + 14$ electron case there is no driving force for reducing the C–C bond length from 2.4 to 1.2 Å. The underlying reason for this can be traced to the e_3 molecular orbitals which become more antibonding as the C–C distance decreases to a greater extent than the e_1 molecular orbitals. These orbitals are represented schematically in Scheme 2 and it is noteworthy that the e_3 molecular orbital is more localised on the carbon atoms than e_1 and therefore experiences a greater effect as a result of a decrease in the C–C distance. It is apparent also from Scheme 2 that the overlap integral between $\pi^\star$ and the e_3 skeletal molecular orbital changes more than that between π and e_1, because the additional nodal plane introduces antibonding interactions between C and the non adjacent ring of gold atoms.

It is evident from the Walsh diagram in Fig. 3 that in $[C_2(AuPH_3)_{10}]^{4+}$ with $12n_s + 14$ valence electrons the preferred geometry for the C_2 moiety is that with the carbon atoms well separated. Calculations of the total energy indicate an energy minimum for the C–C distance at 2.50 Å. The addition of two extra electrons into

the molecular orbital derived from $b_2(\sigma_s^\star)$ leading to $[C_2(AuPH_3)_{10}]^{2+}$ which has $12n_s + 16$ valence electrons leads to a geometry with an even longer C–C distance since this molecular orbital is C–C antibonding (see Scheme 3). It is apparent from the Walsh diagram in Fig. 3 that this molecular orbital rises steeply in energy when the C–C distance is decreased from 2.4 to 1.8 Å, primarily because its C–C anti-bonding character. At shorter distances an avoided crossing diminishes this effect, but not sufficiently to stabilise a geometry with a short C–C distance. The total energy calculations suggest a C–C distance of 3.10 Å for this cluster.

We have also investigated the relative stabilisation energies for $[C_2(AuPH_3)_{10}]^{2+}$ and two isolated $[C(AuPH_3)_5]^+$ molecules, each with a square pyramidal geometry and the carbon atom lying in the square base. The dissociation process

$$\underset{(12n_s+16)}{[C_2(AuPH_3)_{10}]^{2+}} \rightleftharpoons 2\underset{(12n_s+8)}{[C(AuPH_3)_5]^+}$$

is very favourable, and it is unlikely that a dicarbido cluster of this type with well separated carbon atoms would be stable. The gold–gold bonding between the two square-pyramids in the bicapped square antiprism is not sufficiently strong to stabilise such a dicarbido cluster and prevent its dissociation.

The Walsh diagram in Fig. 3 suggests that a dicarbido cluster with a short C–C distance will only be formed if the e_3 molecular orbitals are empty, i.e. for the cluster $[C_2(AuPH_3)_{10}]^{8+}$. Total energy calculations for this electron count $(12n_s + 10)$ confirm this conclusion. The high positive charge associated with the cluster makes it an unrealistic synthetic target, unless some of the phosphine ligands were replaced by anionic halide ligands. Formally such a cluster can be viewed as a derivative of $H_3PAuC{\equiv}CAuPH_3$ with eight capping $AuPH_3^+$ fragments around the C≡C triple bond.

Molecular orbital calculations on $[C_2(AuPH_3)_{12}]^{m+}$ $(m = 6;\ 12n_s + 14;\ m = 4;\ 12n_s + 16)$ with the C_2 moiety inside an icosahedral (or bicapped pentagonal antiprism) gold cluster have also been completed and the basic bonding interactions are very similar to those described above. However, the conclusions regarding the equilibrium C–C distances are rather different. In particular, for the $12n_s + 14$ electron cluster the calculated equilibrium C–C distance is 1.70 Å and for the $12n_s + 16$ electron cluster 2.05 Å. The stabilisation of C_2 moieties with shorter C–C distances in $[C_2(AuPH_3)_{12}]^{m+}$ $(m = 4$ or $6)$ compared with $[C_2(AuPH_3)_{10}]^{m+}$ $(m = 2$ or $4)$ can be related to the following factors. The molecular orbitals which correspond to the $\pi^\star$–$e_3(D^\sigma_{xz,yz})$ in the bicapped square antiprism are $\pi^\star$–$e_{1g}(D^\sigma_{xz,yz})$ in the icosahedron and they become less strongly antibonding as the C–C distance is shortened. This results partly because these molecular orbitals are less localised on the carbon atoms in the larger icosahedral cluster. Also in the icosahedron the carbon atoms can approach each other more closely without losing important bonding interactions with the apical metal atoms. For an icosahedron with Au–Au = 2.80 Å the distance between an apical gold atom and a carbon located at the centre of the adjacent pentagonal plane is 1.47 Å, whereas the corresponding distance in a bicapped square antiprism is 1.98 Å. Since an optimal Au–C distance is approximately 2.0 Å the carbon atoms in the icosahedron can move closer together and still achieve Au–C bond lengths which fall in the usual range.

Calculations have also been completed on $[C_2(AuPH_3)_8]^{m+}$ ($m = 2$; $12n_s + 14$; $m = 0$; $12n_s + 16$) based on two trigonal prisms sharing a square face and $[C_2(AuPH_3)_{12}]^{m+}$ ($m = 6$; $12n_s + 14$; $m = 4$; $12n_s + 16$) based on two square antiprisms sharing a square face and the conclusions are very similar to those developed above.

In summary, the ability to stabilise a C_2 moiety within a gold cluster is intimately connected with the geometric features of the metal polyhedron. A bonded C–C dicarbido cluster will only be formed in a cluster with $12n_s + 14$ valence electrons if the carbon atoms can simultaneously form bonds of ca 2.0 Å to the gold atoms and a C–C bond of 1.2–1.8 Å. The metal icosahedron provides a cavity which satisfies this requirement, but the bicapped square antiprism does not. For clusters with $12n_s + 16$ valence electrons dissociation into a pair of monocarbido clusters with $12n_s + 8$ valence electrons is favoured for both the bicapped square antiprism and the icosahedron. The calculations also indicate the possibility of forming dicarbido clusters with short C–C distances if the total electron count is $12n_s + 10$. A high degree of multiple bond character results from the depopulation of the frontier orbitals in $[C_2(AuPH_3)_{10}]^{4+}$ and $[C_2(AuPH_3)_{12}]^{6+}$ clusters, since these orbitals are C–C antibonding.

Acknowledgements

The SERC is thanked for financial support and Lin Zhenyang for helpful comments. R.P.F.K.'s stay at Oxford was made possible by grants from the Netherlands Foundation for Chemical Research (SON) and the British Council.

References

1 D.M.P. Mingos, J. Chem. Comm., Dalton Trans., (1976) 1163.
2 P. Bellon, M. Manassero, and M. Sansoni, J. Chem. Comm., Dalton Trans., (1973) 2423.
3 F. Scherbaum, A. Grohmann, B. Huber, C. Krüger, and H. Schmidbaur, Angew. Chem., Int. Ed. Engl., 27 (1988) 1544.
4 F. Scherbaum, A. Grohmann, G. Müller, and H. Schmidbaur, Angew. Chem., Int. Ed. Eng., 28 (1989) 463.
5 D.G. Evans and D.M.P. Mingos, J. Organomet. Chem., 232 (1982) 171.
6 D.M.P. Mingos, Proc. Roy. Soc., A, 308 (1982) 25.
7 D.M.P. Mingos and K.P. Hall, Prog. Inorg. Chem., 32 (1982) 239.
8 D.M.P. Mingos, K.P. Hall, and D.I. Gilmour, J. Organomet. Chem., 268 (1984) 275.
9 J.F. Halet and D.M.P. Mingos, Organometallics, 7 (1988) 51.
10 D.J. Wales and D.M.P. Mingos, Inorg. Chem., 28 (1989) 2748.
11 C.E. Briant, K.P. Hall, D.M.P. Mingos, and A.C. Wheeler, J. Chem. Comm., Dalton Trans., (1986) 687.
12 J.F. Halet, D.G. Evans, and D.M.P. Mingos, J. Am. Chem. Soc., 110 (1988) 87, and refs. therein.
13 P.G. Jones, G.M. Sheldrick, R. Uson, and A. Laguna, Acta Cryst., B, 36 (1980) 1486.
14 A.N. Nesmeyanov, E.G. Perevalova, Yu.T. Struchkov, M.Yu. Antipin, K.I. Grandberg, and V.P. Dyadchenko, J. Organomet. Chem., 210 (1980) 343.
15 C. Lensch, P.G. Jones, and G.M. Sheldrick, Z. Naturforsch., B, 37 (1982) 944.
16 Yu.L. Slovokhotov and Yu.T. Struchkov, J. Organomet. Chem., 277 (1984) 143.